

Multiple Chiral Majorana Fermion Modes and Quantum Transport

Jing Wang^{1,2,*} and Biao Lian^{3,†}

¹State Key Laboratory of Surface Physics, Department of Physics, Fudan University, Shanghai 200433, China

²Collaborative Innovation Center of Advanced Microstructures, Nanjing 210093, China

³Princeton Center for Theoretical Science, Princeton University, Princeton, New Jersey 08544, USA

 (Received 18 June 2018; published 19 December 2018)

The chiral Majorana fermion is a massless self-conjugate fermionic particle that could arise as the quasiparticle edge state of a two-dimensional topological state of matter. Here we propose a new platform for a chiral topological superconductor (TSC) in two dimensions with multiple N chiral Majorana fermions from a quantized anomalous Hall insulator in proximity to an s -wave superconductor with nontrivial band topology. A concrete example is that a $N = 3$ chiral TSC is realized by coupling a magnetic topological insulator to the ion-based superconductor such as $\text{FeTe}_{0.55}\text{Se}_{0.45}$. We further propose the electrical and thermal transport experiments to detect the Majorana nature of three chiral edge fermions. A smoking gun signature is that the two-terminal electrical conductance of a quantized anomalous Hall-TSC junction obeys a unique distribution averaged to $(2/3)e^2/h$, which is due to the random edge mode mixing of chiral Majorana fermions and is distinguished from possible trivial explanations. The *homogenous* system proposed here provides an ideal platform for studying the exotic physics of chiral Majorana fermions.

DOI: 10.1103/PhysRevLett.121.256801

The chiral Majorana fermion, a massless fermionic particle which is its own antiparticle, could arise as a one-dimensional quasiparticle edge state of a 2D topological states of matter [1–10]. The non-Abelian braiding of chiral Majorana fermions [11] may be useful in topological quantum computation [12,13]. A simple example of hosting a chiral Majorana fermion mode (CMFM) is the $p_x + ip_y$ chiral topological superconductor (TSC) with a Bogoliubov–de Gennes (BdG) Chern number $N = 1$, which can be realized from a quantum anomalous Hall (QAH) plateau transition in proximity to a conventional s -wave superconductor [14–16], and can be driven by an external magnetic field or electric field in magnetic topological insulators (MTIs) [17–21]. The single CMFM backscattering in a QAH-TSC-QAH (QTQ) junction is predicted to exhibit a half quantized conductance plateau [15,16,22], which has been recently observed in a $\text{Cr}_x(\text{Bi}, \text{Sb})_{2-x}\text{Te}_3$ (CBST) thin film QAH system in proximity with a Nb superconductor [17]. The magnetic field at coercivity inevitably introduces random domains, making MTIs strongly disordered in experiments [23]. The single CMFM in this system is robust against disorder [24]. However, alternative explanations of the half plateau without CMFM under strong disorders have been proposed [25,26], which arises from incoherence due to disorder. Therefore, a homogenous system hosting CMFM and the decisive transport signature are highly desired.

In this Letter, we propose a new platform for an odd Chern number N chiral TSC, which supports multiple CMFMs. The random edge mode mixing of CMFMs leads

to a unique conductance distribution averaged to $(2/3)e^2/h$ in the QTQ junction, which is the smoking gun signature of CMFMs. This is in sharp contrast to the previous proposal that chiral TSC is achieved near the QAH plateau transition [14,16], where strong disorders accompany in the system. Here the system is *homogenous*, which provides an ideal platform for studying the exotic physics of CMFMs.

Model.—The basic mechanism for 2D chiral TSC is to introduce s -wave superconductivity (s -SC) and ferromagnetism (FM) into a strong spin-orbit coupled (SOC) system, such as the spin-helical surface states (SSs) of TIs [27,28]. Instead of inducing superconductivity into a MTI for chiral TSC, one can introduce the FM proximity effect into superconducting Dirac SSs, where the CMFM exists at the boundary between FM and a superconductor [29]. The latter one is more practical for a homogenous system, since FM exchange coupling is usually much larger than s -SC proximity. Therefore, it is natural to ask whether exotic topological states exist in the heterostructure of MTI and an s -SC with nontrivial band topology (dubbed as topological s -SC (T s -SC)), as shown in Fig. 1(a). The T s -SC has a fully bulk pairing gap and an s -SC gap on the single spin-helical Dirac SS. The prototype T s -SC materials are the ion-based superconductors such as $\text{FeTe}_{0.55}\text{Se}_{0.45}$ (FTS) [30]. The general theory presented here for chiral TSC is generic for the higher Chern number QAH insulator [31] and T s -SC. We would like to start with a simple model describing the $C = 1$ QAH in MTIs [32] for concreteness. The low energy physics of the heterostructure is described by four Dirac

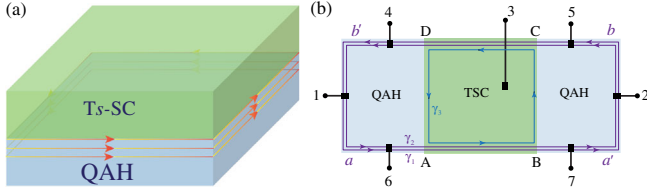


FIG. 1. (a) The heterostructure for chiral TSC with an odd number of CMFMs consists of QAH in MTIs and a Ts-SC on top. Take $C = 1$ QAH e.g., a $N = 3$ TSC is realized when the exchange field is large enough. When QAH has a higher Chern number, a higher odd number N TSC may be realized. (b) The transport configuration of a QTQ ($N-N'-N = 2-3-2$) junction device. The arrows on the edge represent CMFMs.

SSs only, for the bulk states in MTI and Ts-SC are gapped. The generic form of the 2D effective Hamiltonian without superconducting proximity effect is

$$\mathcal{H}(\mathbf{k}) = \begin{pmatrix} H_1 & V \\ V^\dagger & H_2 \end{pmatrix}. \quad (1)$$

Here, H_1 describes the Ts-SC SSs with proximity effect from MTI, the bulk metallic states in Ts-SC are neglected since they are gapped with superconducting pairing, and H_2 describes the QAH in MTI film,

$$H_1 = v_1 k_y \sigma_1 \tau_3 - v_1 k_x \sigma_2 \tau_3 + \frac{\lambda_1}{2} \sigma_3 (1 - \tau_3) + 2\delta, \\ H_2 = v_2 k_y \sigma_1 \tau_3 - v_2 k_x \sigma_2 \tau_3 + m(k) \tau_1 + \lambda_2 \sigma_3, \quad (2)$$

with the basis of $\varphi_{\mathbf{k}}^i = (c_{i\uparrow}, c_{i\downarrow}, c_{b\uparrow}, c_{b\downarrow})^T$, ($i = 1, 2$), where t and b denote the top and bottom SSs and \uparrow and \downarrow represent spin up and down states, respectively. σ_j and τ_j ($j = 1, 2, 3$) are Pauli matrices acting on spin and layer, respectively. v_i is Fermi velocity, which have opposite signs in FTS and MTI [30,33,34]. (The relative sign of velocities do not affect the results). λ_i is an FM exchange field along the z axis that can be tuned by a magnetic field. The short-range FM proximity effect only affects the bottom SS of Ts-SC and $\lambda_1 \leq \lambda_2$. $m(k) = m_0 + m_1 |\mathbf{k}|^2$ is the hybridization between the top and bottom SSs in MTI. $|\lambda_2| > |m_0|$ guarantees a QAH state in MTI. 2δ is the energy band alignment between two Dirac cones. For simplicity, we set $v_2 = -v_1 \equiv v$, $\lambda_1 = \lambda_2 \equiv \lambda$, and neglect the inversion symmetry breaking in each material. $V = g\tau_-$ is the hybridization between the bottom Ts-SC and the top MTI surfaces at interface, where $\tau_- = (\tau_1 - i\tau_2)/2$, g is the real constant.

With superconducting proximity effect, a finite pairing amplitude is induced in MTI and Ts-SC SSs. The BdG Hamiltonian becomes $H_{\text{BdG}} = (1/2) \sum_{\mathbf{k}} \Psi_{\mathbf{k}}^\dagger \mathcal{H}_{\text{BdG}}(\mathbf{k}) \Psi_{\mathbf{k}}$, with $\Psi_{\mathbf{k}} = (\psi_{\mathbf{k}}^T, \psi_{-\mathbf{k}}^\dagger)^T$, $\psi_{\mathbf{k}} = (\varphi_{\mathbf{k}}^1, \varphi_{\mathbf{k}}^2)$, and

$$\mathcal{H}_{\text{BdG}}(\mathbf{k}) = \begin{pmatrix} \mathcal{H}(\mathbf{k}) - \mu & \Delta(\mathbf{k}) \\ \Delta^\dagger(\mathbf{k}) & -\mathcal{H}^*(-\mathbf{k}) + \mu \end{pmatrix}, \\ \Delta(\mathbf{k}) = \begin{pmatrix} \Delta_1(\mathbf{k}) & 0 \\ 0 & \Delta_2(\mathbf{k}) \end{pmatrix}, \quad (3)$$

Here μ is the chemical potential relative to the Dirac cone in MTI, $\Delta_1(\mathbf{k}) = i\Delta_1\sigma_2$, and $\Delta_2(\mathbf{k}) = i(\Delta_2^t/2)\sigma_2(1 + \zeta_3) + i(\Delta_2^b/2)\sigma_2(1 - \zeta_3)$ with ζ_3 as the Pauli matrix in Nambu space. Δ_1 , Δ_2^t , and Δ_2^b are the pairing gap functions in SSs of Ts-SC, top, and bottom MTI. All Δ_i are chosen as \mathbf{k} independent, since they are induced by the s -SC proximity effect, e.g., from the bulk hole pocket at Γ point in an FTS. Usually $\Delta_1 \geq \Delta_2^t \gg \Delta_2^b$. Here we set $\Delta_1 = \Delta_2^t \equiv \Delta$ and $\Delta_2^b = 0$, which is realistic in a superconducting proximity effect between Bi_2Te_3 thin film and FTS with short coherence length [35].

Phase diagram.—The BdG Hamiltonian in Eq. (3) can be classified by the Chern number N . Since the topological invariants cannot change without closing the bulk gap, the phase diagram can be determined by first finding the phase boundaries as gapless regions in parameter spaces, and then calculate N of the gapped phases. We first consider the phase diagram in the limit $g = 0$, in which case the system is decoupled into two BdG models H_1^{BdG} and H_2^{BdG} ,

$$H_i^{\text{BdG}} = \begin{pmatrix} H_i(\mathbf{k}) - \mu & \Delta_i(\mathbf{k}) \\ \Delta_i^\dagger(\mathbf{k}) & -H_i^*(-\mathbf{k}) + \mu \end{pmatrix}. \quad (4)$$

Here H_1^{BdG} is the superconducting Dirac SSs of Ts-SC with only the bottom SS in proximity to FM. The top and bottom SSs in Ts-SC are further decoupled. The energy spectrum of the top SS is $E_{\mathbf{k}}^{1,t} = \pm \sqrt{(\pm v|\mathbf{k}| - \mu')^2 + \Delta^2}$, and $\mu' = \mu - 2\delta$, which resembles that of the spinless $p_x + ip_y$ superconductor but respects time-reversal symmetry [5]. The excitation spectrum of the bottom SS is $E_{\mathbf{k}}^{1,b} = \pm \sqrt{\Delta^2 + \lambda^2 + \mu'^2 + v^2|\mathbf{k}|^2 \pm \sqrt{\lambda^2(\Delta^2 + \mu'^2) + \mu'^2 v^2 |\mathbf{k}|^2}}$, with the gap closing point at $\mathbf{k} = 0$ and $\lambda = \sqrt{\Delta^2 + \mu'^2}$. For $|\lambda| < \sqrt{\Delta^2 + \mu'^2}$, the bottom SS is adiabatically connected to the top SS in the $\lambda = 0$ limit, so they are topologically equivalent. Therefore, the whole Ts-SC SS possesses nontrivial topology, but there is no chiral edge state, since there is no geometric edge to the 2D surface of a 3D bulk. For $|\lambda| > \sqrt{\Delta^2 + \mu'^2}$, the bottom SS is adiabatically connected to FM with $\Delta = \mu' = 0$, which is topologically trivial, so there exists a single CMFM at the edge domain boundary at Ts-SC bottom, and $N_1 = \text{sgn}(\lambda)$ is the sign of λ . H_2^{BdG} is the superconducting proximity coupled QAH insulator, which has been studied in Ref. [16]. For $\mu = 0$, $N_2 = 0$; for $|\lambda| < \lambda_c^-$ (which vanishes when $m_0 = 0$), $N_2 = \text{sgn}(\lambda)$; for $\lambda_c^- < |\lambda| < \lambda_c^+$, and

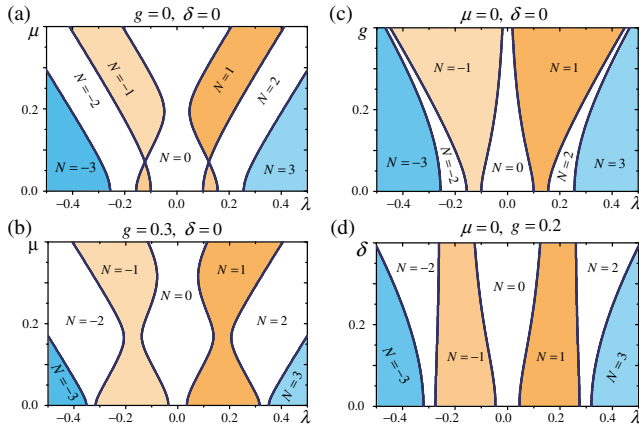


FIG. 2. Phase diagram of the heterostructure with typical parameters. (a) $g=0$, $\delta=0$. (b) $g=0.3$, $\delta=0$. (c) $\mu=0$, $\delta=0$. The even $N=0, 2$ phases disappear when $m_0=0$ and the phase boundary between $N=1$ and $N=3$ is $g=\sqrt{\lambda^2-\Delta^2}$. (d) $\mu=0$, $\delta=-0.1$. All other parameters $v=1$, $\Delta=0.1$, $m_0=0.2$.

$N_2=2\text{sgn}(\lambda)$ for $|\lambda|>\lambda_c^+$. Here $\lambda_c^\pm=(\sqrt{4m_0^2+\Delta^2}\pm\Delta)/2$. A finite μ enlarges the odd N_2 TSC phase. The total Chern number of the heterostructure without V is $N=N_1+N_2$. The phase diagram with parameters (μ, λ) is shown in Fig. 2(a), where different chiral TSC phases are denoted by the corresponding Chern numbers.

Next, we study the effect of V at interface. Similar to the $g=0$ case, we determine the phase boundaries by gapless regions in Eq. (3), which is always at $\mathbf{k}=0$ point. Therefore, any \mathbf{k} -dependent pairing [36,37] will not affect the phase diagrams. As shown in Fig. 2(b), when the g term is turned on, it makes the chiral TSC phase with the same Chern numbers simply connected. Meanwhile, it shrinks the $N=0$ phase and enlarges the $N=1$ phase, and further pushes the phase boundary between $N=2$ and $N=3$ towards a larger λ . For a given exchange field, μ will drive the system into TSC phases with smaller N . Therefore, one optimal condition for $N=3$ TSC is $\mu=0$, which corresponds to an undoped QAH system. This is just the opposite to the optimal condition $\mu\neq 0$ for obtaining the $N=1$ TSC phase from QAH plateau transition [16]. As shown in Fig. 2(c), g enlarges the $N=1$ phase and shrinks all other N phases. This can be understood from the band crossing at the interface. The single-particle Hamiltonian at the interface is $H_{\text{int}}=vk_y\sigma_1-vk_x\sigma_2+\lambda\sigma_3+g\tau_1+\delta(1+\tau_3)$, with the energy spectrum $E_{\text{int}}=\delta\pm(\sqrt{g^2+\delta^2}\pm\sqrt{\lambda^2+v|\mathbf{k}|^2})$. g splits the two copies of Dirac bands up and down in energy. Whenever the Dirac band edge crosses the chemical potential, N reduces by one. As shown in Fig. 2(d), δ enlarges the trivial even N TSC, and shrinks the nontrivial odd N TSC towards larger λ . Similarly, m_0 enlarges $N=0$ TSC and shrinks $N\neq 0$ TSC. Thus $m_0=\delta=0$ is preferred for a higher N TSC. For a simple case $m_0=\delta=0$ and infinitesimal Δ , a simple sum rule for the Chern number of the heterostructure is

$$N=N_2+\text{sgn}(|\lambda|-|g|)N_1. \quad (5)$$

In general, the coupling g will strongly modify the Chern number of the heterostructure from that of the decoupled systems. The chiral TSC with higher odd Chern numbers requires a large enough exchange field, and is simply obtained by growing the multilayer heterostructure or by using a higher Chern number QAH following the above recipe.

Transport.—To probe the multiple neutral CMFMs, we consider the electrical and thermal transports in an $N=3$ chiral TSC. The Hall bar device we shall discuss is a QTQ junction as shown in Fig. 1(b), which has been studied for $N=1$ and $N=2$ chiral TSCs. Both the left and right QAH regions have a Chern number $C=1$, and thus have a charged chiral fermion mode on their edges with a vacuum. The charge chiral fermion mode can be equivalently written as two CMFMs, γ_1 and γ_2 , as shown in Fig. 1(b), and the electron annihilation operators a, a', b, b' on the left (right) bottom (top) QAH edges are locally related to the CMFMs as $a, a', b, b'=\gamma_1+i\gamma_2$. There exists a third CMFM γ_3 on the vertical edges between $C=1$ QAH and $N=3$ TSC, which merges with γ_1 and γ_2 on the top and bottom TSC edges.

We assume the current is only applied at terminals 1, 2, and 3, while terminals 4 to 7 are only used as voltage leads. The lead on electrode 3 is connected to the TSC bulk, while all the other leads are on the edge. The electrical transport of the superconducting junction is governed by the generalized Landauer-Büttiker formula [15,16,38,39], which takes the form among leads 1–3 as

$$\begin{aligned} I_1 &= \frac{e^2}{h} [(1-r+r^A)(V_1-V_s) + (t-t^A)(V_s-V_2)], \\ I_2 &= \frac{e^2}{h} [(1-r+r^A)(V_2-V_s) + (t-t^A)(V_s-V_1)], \\ I_3 &= -I_1 - I_2, \quad V_3 = V_s, \end{aligned} \quad (6)$$

where I_i and V_i are the inflow current and voltage of lead i , V_s is the voltage of the TSC, and we have assumed the contact resistance vanishes between lead 3 and the TSC bulk, which is appropriate when the electrodes are good metals. Here r, r^A, t , and t^A are the normal reflection, Andreev reflection, normal transmission, and Andreev transmission probabilities between leads 1 and 2, respectively, satisfying $r+r^A+t+t^A=1$.

To examine the normal and Andreev probabilities, consider the charged chiral fermion mode $a=\gamma_1+i\gamma_2$ incident from lead 1. When propagating on the bottom TSC edge $A-B$, it could randomly mix with γ_3 due to unavoidable edge disorders. Therefore, when the incident charge mode a reaches corner B , it has the normal and Andreev probabilities t_1 and t_1^A to become a' and a'^{\dagger} , but also has a remaining probability $p^{(1)}=1-t_1-t_1^A$ to propagate as γ_3 .

The γ_3 mode will then circulate along the TSC edge, and has a propagation probability into charge modes b' , b'^{\dagger} (or a' , a'^{\dagger}) whenever it reaches corner D (or B), thus contributing probabilities r_n and r_n^A (or t_n and t_n^A) during its n th lap. Summing over n then yields the total r , r^A , t , and t^A . Such a summation is difficult. However, since γ_3 is charge neutral, its propagation probability into electron and hole states will always be equal, so we conclude that $r_n = r_n^A$ for any n , and $t_n = t_n^A$ for all $n \geq 2$. Therefore, we find $t - t^A = t_1 - t_1^A$, and $r - r^A = 0$, which are the only quantities needed in Eq. (6). Quite different from the interference [29,40–43], here we assume that the system size is large, so that the CMFMs lose coherence during their propagations.

Next we calculate $t_1 - t_1^A$. The chemical potential, hopping, and pairing on TSC edge A – B yields a term $H_R = i\gamma^T L(x)\gamma$ in the Hamiltonian, where $\gamma = (\gamma_1, \gamma_2, \gamma_3)^T$ is the CMFM basis, and $L(x)$ is a 3×3 real antisymmetric matrix. In terms of the $SO(3)$ group generators $\mathbf{T} = (T_1, T_2, T_3)$, one can rewrite it as $L = i\omega \mathbf{n} \cdot \mathbf{T}$, where $|\mathbf{n}| = 1$. For a given edge, one expects $\omega = \langle \omega \rangle + \delta\omega(x)$ and $\mathbf{n} = \langle \mathbf{n} \rangle + \delta\mathbf{n}(x)$ to fluctuate, where we assume the fluctuations $|\delta\mathbf{n}(x)| \ll |\langle \mathbf{n} \rangle|$. This leads to a $SO(3)$ transformation $Q \approx e^{i\phi(\mathbf{n})\mathbf{T}}$ of γ , where $\phi \approx \int_A^B \omega(x) dx / v_M$ is uniformly random in $[0, 2\pi)$ when edge A – B is longer than the dephasing length (due to thermal noise, etc.), and v_M is the average Majorana velocity [44–46]. The Majorana velocity anisotropy leads a deviation of Q away from $SO(3)$ [22], but the deviation is irrelevant in long distances [47,48]. The average normal and Andreev transmissions along the edge are thus the mean value over ϕ :

$$t_1 = \overline{|u^{\dagger} Q u|^2}, \quad t_1^A = \overline{|u^T Q u|^2}, \quad (7)$$

where $u = (1, i, 0)^T / \sqrt{2}$ is the electron annihilation operator under the Majorana basis. The result gives $t_1 - t_1^A = \cos^2 \theta$, where θ is the angle between $\langle \mathbf{n} \rangle$ and the γ_3 axis (see the Supplemental Material [47]). By defining $\sigma_{12} = I / (V_1 - V_2)$ for the current $I = I_1 = -I_2$ applied between leads 1 and 2 ($I_3 = 0$), and $\sigma_{13} = I / (V_1 - V_3)$ for the current $I = I_1 = -I_3$ applied at leads 1 and 3 ($I_2 = 0$), we obtain $\sigma_{12} = (1 + \cos^2 \theta) / 2$ and $\sigma_{13} = 1 - \cos^4 \theta$ in units of e^2/h . Note that $\langle \mathbf{n} \rangle$ depends on samples and physical conditions, so if we assume that $\langle \mathbf{n} \rangle$ distributes uniformly on the unit sphere S^2 , we obtain the probability distributions of σ_{12} and σ_{13} among various samples or physical conditions

$$p(\sigma_{12}) = \frac{1}{\sqrt{2\sigma_{12} - 1}}, \quad p(\sigma_{13}) = \frac{1}{4(1 - \sigma_{13})^{3/4}}, \quad (8)$$

where $\sigma_{12} \in [\frac{1}{2}, 1]$ and $\sigma_{13} \in [0, 1]$ in units of e^2/h . The average values of σ_{12} and σ_{13} can then be derived to be $\bar{\sigma}_{12} = (2/3)e^2/h$ and $\bar{\sigma}_{13} = (4/5)e^2/h$. Moreover, if the TSC edge is in the strong fluctuation limit $|\delta\mathbf{n}(x)| \gg |\langle \mathbf{n} \rangle|$

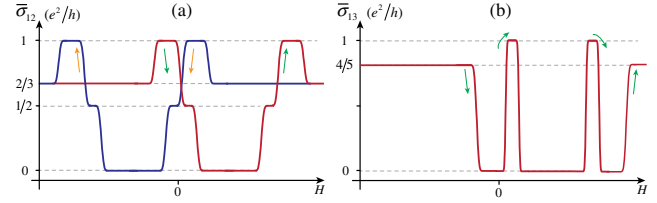


FIG. 3. (a) The average value $\bar{\sigma}_{12}$ generically shows a plateau transition $2/3 \rightarrow 1 \rightarrow 1/2 \rightarrow 0 \rightarrow 1/2 \rightarrow 1 \rightarrow 2/3$ in units of e^2/h during the hysteresis loop. (b) The average value $\bar{\sigma}_{13}$ shows $4/5$ and 1 peaks for $|N| = 3$ and $|N| = 1$ TSC phases, respectively. Here only one cycle of hysteresis loop is shown.

(induced by strong static disorders, etc.), we would have $t = t^A$, leading to quantized conductances $\sigma_{12} = e^2/2h$ and $\sigma_{13} = e^2/h$ [47]. For disorders that affect both bulk and edge, the bulk may undergo disorder-driven phase transitions before the edge disorder reaches the strong limit, in which case the strong limit results here will not be reached.

In addition, the resistance matrix measured from other leads are $R_{12,46} = R_{12,57} = h/e^2$, and $R_{12,45} = R_{12,67} = \sigma_{12}^{-1} - h/e^2$, where $R_{ij,kl} \equiv (V_k - V_l)/I$ with the current I applied between leads i and j [47].

The exchange field can be tuned by either a perpendicular or an in-plane external magnetic field. Therefore, the TSC phases will experience the BdG Chern number variation $N = 3 \rightarrow 2 \rightarrow 1 \rightarrow 0 \rightarrow -1 \rightarrow -2 \rightarrow -3$ as λ decreases in the hysteresis loop. Meanwhile, the QAH phase will experience the Chern number change $C = 1 \rightarrow 0 \rightarrow -1$, and in terms of $N = 2 \rightarrow 0 \rightarrow -2$. In general, the average $\bar{\sigma}_{12}$ will exhibit the plateau transition as shown in Fig. 3(a). Since the system in the magnetized state without external magnetic fields is homogenous in the sense of weak disorder without percolation transition, the unique $2/3$ quantized average conductance plateau manifests the $N = 3$ TSC.

Finally, we discuss the thermal transport. The $N = 3$ chiral TSC exhibits a quantized thermal Hall conductance $\kappa_{xy}/T = 3$ in units of $\kappa_0 = (\pi^2/6)(k_B^2/h)$, with k_B (the Boltzmann constant) and T (temperature). Moreover, the QTQ junction will exhibit quantized thermal resistances resembling the electric resistances of a filling factor 2-3-2 integer quantum Hall junction [49,50]. For a heat current applied between leads 1 and 2, the thermal resistances are given by $R_{12,46}^Q = R_{12,57}^Q = 1/2$, and $R_{12,45}^Q = R_{12,67}^Q = 1/6$ in units of $1/(\kappa_0 T)$. Here the full thermal equilibration among the CMFMs is assumed. The phonon and magnon contributions can be eliminated from the temperature dependence [51].

We discuss the experimental feasibility of the proposed state. The key point is to invert the bands by a large exchange field, while keeping the QAH insulating. The hybridization between top and bottom SSs in QAH is better to be small. For QAH in MTIs, $\lambda \approx 30$ meV in CBST [52], and $\lambda \approx 50$ meV in V-I codoped-TI [53]. m_0 vanishes when

film thickness exceeds five quintuple layers. For Ts-SC in FTS, $\Delta = 2$ meV and $\mu = 5$ meV below $T_c = 14.5$ K [30]. The work functions in FTS and $(\text{Bi, Sb})_2\text{Te}_3$ thin film grown on SrTiO_3 are almost the same as about 4.3 ± 0.1 eV; thus δ can be tuned to be small [54]. g is unknown, but can be tuned by inserting an insulating ultrathin layer such as CdSe between Ts-SC and QAH. Other possible Ts-SC materials include an ion-based superconductor such as BaFe_2As_2 and LiFeAs [55], and the superconducting doped TIs such as $\text{Cu}_x\text{Bi}_2\text{Se}_3$ and $\text{Tl}_x\text{Bi}_2\text{Te}_3$ [56–58]. Recently, the QAH with higher Chern numbers has been realized in a multilayer of MTI [59]. Such experimental progress on the material growth and rich material choice of MTI and Ts-SC makes the realization of the higher odd N chiral TSC feasible.

In summary, the random mode mixing of CMFMs leads to unique quantum transport, which can be served as a smoking gun signature of the Majorana nature of chiral edge fermions. The coherent mixing of the CMFMs leads to nontrivial interference effect and may find applications in topological quantum computation, which is left for future work.

We thank Yang Feng, Xiao Feng, Tong Zhang, and Ke He for helpful discussions. J. W. is supported by the Natural Science Foundation of China through Grant No. 11774065; the National Key Research Program of China under Grant No. 2016YFA0300703; the Natural Science Foundation of Shanghai under Grant No. 17ZR1442500; the National Thousand-Young-Talents Program; the Open Research Fund Program of the State Key Laboratory of Low-Dimensional Quantum Physics through Contract No. KF201606; and by Fudan University Initiative Scientific Research Program. B. L. is supported by the Princeton Center for Theoretical Science at Princeton University.

* wjingphys@fudan.edu.cn

† biao@princeton.edu

- [1] G. Moore and N. Read, *Nucl. Phys.* **B360**, 362 (1991).
- [2] N. Read and D. Green, *Phys. Rev. B* **61**, 10267 (2000).
- [3] A. P. Mackenzie and Y. Maeno, *Rev. Mod. Phys.* **75**, 657 (2003).
- [4] A. Kitaev, *Ann. Phys. (Amsterdam)* **321**, 2 (2006).
- [5] L. Fu and C. L. Kane, *Phys. Rev. Lett.* **100**, 096407 (2008).
- [6] J. D. Sau, R. M. Lutchyn, S. Tewari, and S. D. Sarma, *Phys. Rev. Lett.* **104**, 040502 (2010).
- [7] J. Alicea, *Phys. Rev. B* **81**, 125318 (2010).
- [8] X.-L. Qi, T. L. Hughes, S. Raghu, and S.-C. Zhang, *Phys. Rev. Lett.* **102**, 187001 (2009).
- [9] F. Wilczek, *Nat. Phys.* **5**, 614 (2009).
- [10] S. R. Elliott and M. Franz, *Rev. Mod. Phys.* **87**, 137 (2015).
- [11] B. Lian, X.-Q. Sun, A. Vaezi, X.-L. Qi, and S.-C. Zhang, *Proc. Natl. Acad. Sci. U.S.A.* **115**, 10938 (2018).
- [12] A. Kitaev, *Ann. Phys. (Amsterdam)* **303**, 2 (2003).
- [13] C. Nayak, S. H. Simon, A. Stern, M. Freedman, and S. D. Sarma, *Rev. Mod. Phys.* **80**, 1083 (2008).
- [14] X.-L. Qi, T. L. Hughes, and S.-C. Zhang, *Phys. Rev. B* **82**, 184516 (2010).
- [15] S. B. Chung, X.-L. Qi, J. Maciejko, and S.-C. Zhang, *Phys. Rev. B* **83**, 100512 (2011).
- [16] J. Wang, Q. Zhou, B. Lian, and S.-C. Zhang, *Phys. Rev. B* **92**, 064520 (2015).
- [17] Q. L. He, L. Pan, A. L. Stern, E. C. Burks, X. Che, G. Yin, J. Wang, B. Lian, Q. Zhou, E. S. Choi, K. Murata, X. Kou, Z. Chen, T. Nie, Q. Shao, Y. Fan, S.-C. Zhang, K. Liu, J. Xia, and K. L. Wang, *Science* **357**, 294 (2017).
- [18] J. Wang, B. Lian, and S.-C. Zhang, *Phys. Rev. B* **89**, 085106 (2014).
- [19] X. Kou, L. Pan, J. Wang, Y. Fan, E. S. Choi, W.-L. Lee, T. Nie, K. Murata, Q. Shao, S.-C. Zhang, and K. L. Wang, *Nat. Commun.* **6**, 8474 (2015).
- [20] Y. Feng, X. Feng, Y. Ou, J. Wang, C. Liu, L. Zhang, D. Zhao, G. Jiang, S.-C. Zhang, K. He, X. Ma, Q.-K. Xue, and Y. Wang, *Phys. Rev. Lett.* **115**, 126801 (2015).
- [21] J. Wang, *Phys. Rev. B* **94**, 214502 (2016).
- [22] B. Lian, J. Wang, and S.-C. Zhang, *Phys. Rev. B* **93**, 161401 (2016).
- [23] K. Yasuda, M. Mogi, R. Yoshimi, A. Tsukazaki, K. S. Takahashi, M. Kawasaki, F. Kagawa, and Y. Tokura, *Science* **358**, 1311 (2017).
- [24] B. Lian, J. Wang, X.-Q. Sun, A. Vaezi, and S.-C. Zhang, *Phys. Rev. B* **97**, 125408 (2018).
- [25] W. Ji and X.-G. Wen, *Phys. Rev. Lett.* **120**, 107002 (2018).
- [26] Y. Huang, F. Setiawan, and J. D. Sau, *Phys. Rev. B* **97**, 100501 (2018).
- [27] M. Z. Hasan and C. L. Kane, *Rev. Mod. Phys.* **82**, 3045 (2010).
- [28] X.-L. Qi and S.-C. Zhang, *Rev. Mod. Phys.* **83**, 1057 (2011).
- [29] L. Fu and C. L. Kane, *Phys. Rev. Lett.* **102**, 216403 (2009).
- [30] P. Zhang, K. Yaji, T. Hashimoto, Y. Ota, T. Kondo, K. Okazaki, Z. Wang, J. Wen, G. D. Gu, H. Ding, and S. Shin, *Science* **360**, 182 (2018).
- [31] J. Wang, B. Lian, H. Zhang, Y. Xu, and S.-C. Zhang, *Phys. Rev. Lett.* **111**, 136801 (2013).
- [32] C.-Z. Chang *et al.*, *Science* **340**, 167 (2013).
- [33] Z. Wang, P. Zhang, G. Xu, L. K. Zeng, H. Miao, X. Xu, T. Qian, H. Weng, P. Richard, A. V. Fedorov, H. Ding, X. Dai, and Z. Fang, *Phys. Rev. B* **92**, 115119 (2015).
- [34] X. Wu, S. Qin, Y. Liang, H. Fan, and J. Hu, *Phys. Rev. B* **93**, 115129 (2016).
- [35] M. Chen, X. Chen, H. Yang, Z. Du, and H.-H. Wen, *Sci. Adv.* **4**, eaat1084 (2018).
- [36] A. M. Black-Schaffer and A. V. Balatsky, *Phys. Rev. B* **88**, 104514 (2013).
- [37] Z. Faraei and S. A. Jafari, *Phys. Rev. B* **96**, 134516 (2017).
- [38] M. P. Anantram and S. Datta, *Phys. Rev. B* **53**, 16390 (1996).
- [39] O. Entin-Wohlman, Y. Imry, and A. Aharony, *Phys. Rev. B* **78**, 224510 (2008).
- [40] G. Strübi, W. Belzig, M.-S. Choi, and C. Bruder, *Phys. Rev. Lett.* **107**, 136403 (2011).
- [41] Y.-H. Li, J. Liu, H. Liu, H. Jiang, Q.-F. Sun, and X. C. Xie, *Phys. Rev. B* **98**, 045141 (2018).

- [42] A. R. Akhmerov, J. Nilsson, and C. W. J. Beenakker, *Phys. Rev. Lett.* **102**, 216404 (2009).
- [43] K. T. Law, P. A. Lee, and T. K. Ng, *Phys. Rev. Lett.* **103**, 237001 (2009).
- [44] M. Levin, B. I. Halperin, and B. Rosenow, *Phys. Rev. Lett.* **99**, 236806 (2007).
- [45] S.-S. Lee, S. Ryu, C. Nayak, and M. P. A. Fisher, *Phys. Rev. Lett.* **99**, 236807 (2007).
- [46] B. Lian and J. Wang, *Phys. Rev. B* **97**, 165124 (2018).
- [47] See Supplemental Material at <http://link.aps.org/supplemental/10.1103/PhysRevLett.121.256801> for technical details.
- [48] B. Lian and J. Wang, [arXiv:1807.03943](https://arxiv.org/abs/1807.03943).
- [49] J. R. Williams, L. DiCarlo, and C. M. Marcus, *Science* **317**, 638 (2007).
- [50] B. Özyilmaz, P. Jarillo-Herrero, D. Efetov, D. A. Abanin, L. S. Levitov, and P. Kim, *Phys. Rev. Lett.* **99**, 166804 (2007).
- [51] M. Banerjee, M. Heiblum, A. Rosenblatt, Y. Oreg, D. E. Feldman, A. Stern, and V. Umansky, *Nature (London)* **545**, 75 (2017).
- [52] I. Lee, C. K. Kim, J. Lee, S. J. L. Billinge, R. Zhong, J. A. Schneeloch, T. Liu, T. Valla, J. M. Tranquada, G. Gu, and J. C. S. Davis, *Proc. Natl. Acad. Sci. U.S.A.* **112**, 1316 (2015).
- [53] S. Qi, Z. Qiao, X. Deng, E. D. Cubuk, H. Chen, W. Zhu, E. Kaxiras, S. B. Zhang, X. Xu, and Z. Zhang, *Phys. Rev. Lett.* **117**, 056804 (2016).
- [54] Y. Feng (private communication).
- [55] P. Zhang *et al.*, *Nat. Phys.*, DOI: 10.1038/s41567-018-0280-z (2018).
- [56] Y. S. Hor, A. J. Williams, J. G. Checkelsky, P. Roushan, J. Seo, Q. Xu, H. W. Zandbergen, A. Yazdani, N. P. Ong, and R. J. Cava, *Phys. Rev. Lett.* **104**, 057001 (2010).
- [57] L. Fu and E. Berg, *Phys. Rev. Lett.* **105**, 097001 (2010).
- [58] Z. Wang, A. A. Taskin, T. Frlich, M. Braden, and Y. Ando, *Chem. Mater.* **28**, 779 (2016).
- [59] G. Jiang, Y. Feng, W. Wu, S. Li, Y. Bai, Y. Li, Q. Zhang, L. Gu, X. Feng, D. Zhang, C. Song, L. Wang, W. Li, X.-C. Ma, Q.-K. Xue, Y. Wang, and K. He, *Chin. Phys. Lett.* **35**, 076802 (2018).